Model-based Formal Reliability Analysis of Grid Dynamics with Solar Energy Sources

Andrea Peruffo[1], Emeline Guiu[2], Patrick Panciatici[2], and Alessandro Abate[1]

[1] Department of Computer Science, University of Oxford, Oxford, OX1 3QD
{name.surname}@cs.ox.ac.uk,
[2] RTE France, La Defense, Paris, France
{name.surname}@rte-france.com.

Abstract. This work presents a model-based formal reliability analysis of the electricity grid dynamics in the presence of a large population of solar panels, under several scenarios of load demand and of renewables penetration. The electric network is represented as a feedback interconnection between the dynamics of the grid and those of a heterogeneous population of solar panels that injects power into the network. Introducing a formal abstraction technique, we obtain a Markov model that allows to quantitatively verify a reliability specification by means of probabilistic model checking. This specification ensures that the network frequency does not deviate from a reference level following a generation-loss incident. We further encode the population heterogeneity, the total load of the network, and the penetration of solar sources as parameters of the model, and present a procedure to automatically synthesise their values in order to guarantee the reliable operation of the network.

Keywords: grid dynamics, solar panels, reliability analysis, formal abstractions, quantitative model checking, probabilistic safety

1 Introduction

Academia, industry and general public alike have shown an increasing interest in environmental conservation, sustainability issues and, in particular, in the growing presence of energy production by renewables. The installation and growth of hydroelectric, wind and solar energy represents an ever growing trend [1–3]. In this work we account for solar populations, with particular attention to households rooftop devices: such populations are naturally prone to heterogeneity, in view of diverse panel sizes, makes and ages, of standing weather conditions, etc. The main focus of this work is to provide the first formal analysis of renewable energy integration, and to elucidate the relationship between the panels operation and the overall reliability of the electric network. The models we employ are drawn from [4–6], which are based on a physical description of the behaviour of solar devices [7, 8]. These models allow us to precisely forecast the grid dynamics in the presence of a heterogeneous PV population, and to quantify the consequence of generation-loss incidents, under several scenarios of network load

and of population dynamics. We particularly focus on incidents related to *load-shedding*, an automated process that is set in place to mitigate the lack of balance on the network, and to prevent potential subsequent blackouts.

Reliability is a critical aspect of power grids, particularly when investigating smart grids: network resilience is thus studied with several approaches, from simulation-based tests to analytical methods. The work in [9] studies the reliability of smart grids in terms of demand-response programs, renewable energy sources, storage devices and electric vehicles: the authors focus on accommodating cybersecurity measures. A series of reliability indices are introduced in [10] to quantify the performance of solar devices, considering variation of input power and failure rates of critical components. [11] investigates via simulations potential cascading failures, in order to assess the duration before a failure occurs and the consequent recovery phase. The work in [12] draws a framework for future smart grids and assess its reliability with a range of stochastic generation/consumption patterns. Formal verification provides powerful tools to assess quantitative properties, such as reliability, on complex systems, such as the power grid. In [13] the high-level reliability of power systems is tested via fault-tree analysis. The work in [14] presents models of power grids with a significant penetration of solar generation: these models are employed to investigate runtime control algorithms for photovoltaic micro-generators, towards grid stability. Within the arsenal of formal verification, formal abstractions are techniques to approximate complex models by simpler ones that can be easily verified. Unlike the aforementioned literature, we newly extend a formal abstraction procedure [15] to generate parametric models of populations of solar panels interconnected to the grid. We then synthesise parameters corresponding to models that verify properties of interest, related to the safe operation of the grid. In [16] a Markov model is constructed as the aggregation of an inhomogeneous population of thermostatically controlled loads (TCLs). As discussed in [17], the aggregation of population models introduces two kinds of errors: the abstraction error (over a single device) and an error related to the population heterogeneity. By means of a similar approach, in this work we formally abstract the model of a heterogeneous population of PV panels interconnected to the grid as a parametric, finite-state, discrete-time Markov chain (dtMC). The proposed abstraction procedure can be refined to improve its accuracy: the error decreases to zero as the number of generated abstract states increases.

In practice, one is often not only interested in verifying a given model (e.g., via model checking algorithms), but rather in the harder problem of deriving model parameters ensuring the validity of the property under consideration [18, 19]. In this paper, we perform parametric model checking, namely we check whether a property (specifically, the reliability of the electric network) holds under different values of the parameters: we consider the heterogeneity of the solar population, the total load of the network, and the solar penetration level as the tuneable parameters that can ensure a reliable integration of solar devices in the grid dynamics. Among others, tools like PRISM [20], MODEST [21], FAUST^2 [22] and StocHy [23] can be used to perform parametric model check-

ing and formal abstraction. This paper extends earlier results [4–6] by employing techniques from formal verification and parameter synthesis: we tailor a formal abstraction procedure to generate parametric Markov models, and tapping into existing verification software, we formally synthesise model parameters verifying the property of interest (network reliability). We consequently to provide certificates on the safe and reliable operation of the grid under diverse scenarios: these certificates can be relevant for operators of large transmission networks or of smart grids.

The remainder of the paper is organised as follows. Section 2 introduces the solar panel behaviour, its description as a dynamical system, and the overall electric network model. Section 3 discusses the formal abstraction techniques, state space partitioning, and computes the formal synthesis of parameters. Section 4 presents the generation-loss incident scenario and shows test results. Finally, conclusions are drawn in Section 5.

2 Feedback Model of the Electricity Grid and of a Population of Solar Panels

The qualitative description of a single panel operation and the modelling of a population as a Markov model is reported in Section 2.1, whereas Section 2.2 presents the model for the electricity grid and describes the feedback connection between grid and solar panels.

2.1 Model of Solar Panels as a Function of Grid Frequency

We start presenting the qualitative operations of a single photovoltaic panel, which depend on the electricity grid frequency measurements [7, 8].

A panel-inverter is connected to the electric network and samples the frequency $f(k)$, $k \in \mathbb{N}$, where k represents discrete time. According to this measurement, the device can be either connected or disconnected. Regulations impose such devices to be connected to the electricity grid exclusively when $f(k)$ belongs to a safe interval $\mathcal{I}_f$ (a neighbourhood of the nominal frequency $f_0 = 50$ Hz) for a predefined amount of time τ_r. Whilst disconnection is instantaneous, reconnection must wait for τ_r time instants, during which $f(k)$ must vary within $\mathcal{I}_f$. Table 1 summarises the behaviour of a PV panel. This mechanism prevents panels to inject power in a islanding network, namely when part of the grid is disconnected from the rest of it, and also prevents chattering related to rapid connection and disconnection. Note that, when considering a large population of devices, $\mathcal{I}_f$ and τ_r are not homogeneous. In this work we assume that heterogeneous $\mathcal{I}_f$ and τ_r belong to known distributions, as suggested by industrial experts, which more generally can be inferred from data on actual devices.

We now introduce a formal definition of a discrete-time Markov chain, which is the model underpinning the system under consideration.

Definition 1 (dtMC). *A discrete-time Markov chain is a tuple $D = (\mathcal{S}, s_0, P)$ where $\mathcal{S}$ is a finite set of states, $s_0 \in \mathcal{S}$ is an initial state, and $P : \mathcal{S} \times \mathcal{S} \to [0, 1]$ is a transition probability matrix, such that for all $s \in \mathcal{S}$, $\sum_{s' \in \mathcal{S}} P(s, s') = 1$.*

State $q(k)$	Frequency measurement	Delay	State $q(k+1)$
OFF	$f(k) \in \mathcal{I}_f$	$\tau(k) \geq \tau_r$	ON
ON	$f(k) \in \mathcal{I}_f$	–	ON
ON	$f(k) \notin \mathcal{I}_f$	–	OFF
OFF	$f(k) \in \mathcal{I}_f$	$\tau(k) < \tau_r$	OFF

Table 1: Switching behaviour of a single PV panel. The network frequency is $f(\cdot)$, $\tau(\cdot)$ is the internal counter, τ_r the reconnection delay, and k the time index.

The heterogeneity in $\mathcal{I}_f$ and in τ_r allows us to develop a model of the population of solar devices: differences in disconnection and reconnection settings translate into a time-varying Markov model. Formally, as depicted in Fig. 1, we identify three operational states: (1). active (ON, for panels sampling $f(k) \in \mathcal{I}_f$ and for which $\tau(k) \geq \tau_r$); (2). inactive (OFF, for panels sampling $f(k) \notin \mathcal{I}_f$); (3). waiting for reconnection (WAIT, for panels sampling $f(k) \in \mathcal{I}_f$ but $\tau(k) < \tau_r$).

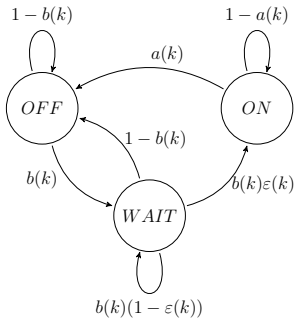

Fig. 1: A (time-varying) Markov model for the aggregated dynamics of a heterogeneous population of solar panels.

The transitions probabilities $a(k)$ and $b(k)$ between the three states are time-varying functions of $f(k)$. They characterise a Markov chain model with the following dynamics:

$$\begin{cases} x(k+1) = (1 - a(k))x(k) + b(k)\varepsilon(k)y(k) \\ y(k+1) = b(k)(1 - x(k) - \varepsilon(k)y(k)), \end{cases} \tag{1}$$

where $x(k)$ and $y(k)$ represent the probability (that is, the portion of panels) of being in the ON and WAIT state at time k, respectively. A new quantity $z(k)$, the probability of being in the OFF state, can be obtained as $1 - x(k) - y(k), \forall\, k$. The function $\varepsilon(k)$ is a time-varying term accounting for the heterogeneity of τ_r. Its form can be inferred from frequency values, as shown in [4]. The quantities

$a(k)$ and $b(k)$ are functions of $f(k)$ as

$$a(k) = \begin{cases} \int_{-\infty}^{f(k)} p_o^d(u)du & \text{if } f(k) > f_0 \\ \int_{f(k)}^{+\infty} p_u^d(u)du & \text{otherwise,} \end{cases}$$

$$b(k) = \begin{cases} \int_{f(k)}^{\infty} p_o^r(u)du & \text{if } f(k) > f_0 \\ \int_{-\infty}^{f(k)} p_u^r(u)du & \text{otherwise,} \end{cases}$$

where p_i^j, $i = \{u, o\}$, $j = \{d, r\}$ are probability distributions describing the population heterogeneity over the intervals $\mathcal{I}_f$: the superscript u and o indicate the under-frequency ($f(k) \leq f_0$) and over-frequency ($f(k) > f_0$) scenarios, respectively, whereas the indices d and r refer to the disconnection and reconnection distributions, respectively. Whilst $a(\cdot)$ and $b(\cdot)$ are functions of the frequency signal $f(k)$, to ease the notation we will denote them as $a(k)$. Fig. 2 depicts an example of the computation of $a(k)$ in under-frequency and over-frequency. These quantities affect the reconnection and disconnection of devices: a more heterogeneous population corresponds to $a(k)$ and $b(k)$ with a higher variance, while a homogeneous population shows smaller variance.

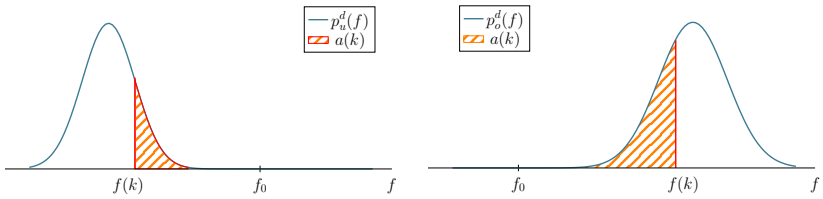

Fig. 2: Pictorial representation of $a(k)$ in over-frequency, i.e. $f(k) > f_0$ (right) and in under-frequency, i.e. $f(k) < f_0$ (left). The value of $f(k)$ is indicated as a red vertical line, which defines the upper or lower integration extrema in over- and under-frequency, respectively. In general p_u and p_o might not be symmetric with respect to f_0, nor belong to the same distribution family.

Assume, for simplicity, that p_i^j, $i \in \{u, o\}$, $j \in \{d, r\}$, are shaped according to a uniform distribution, i.e. $p_i^j \in \mathcal{U}(\mu_i^j, \varsigma_i^j)$, where μ_i^j is the average value and ς_i^j is the variance. The choice of a uniform distribution describes a population of devices in which parameters belong to an admissible range, with no further assumptions. Define the domain of p_i^j as $\Lambda_i^j = [\lambda_{i,1}^j, \lambda_{i,2}^j]$. We now focus on the under-frequency disconnection scenario: other settings (i.e. under-frequency

reconnection and over-frequency disconnection/reconnection) allow for similar conclusions. Since $p_u^d \in \mathcal{U}(\mu_u^d, \varsigma_u^d)$, $a(k)$ is a piecewise linear function, namely

$$a(k) = \begin{cases} 0 & f(k) < \lambda_{u,1}^d \\ \kappa f(k) - q & f(k) \in \Lambda_u^d \\ 1 & f(k) > \lambda_{u,2}^d, \end{cases}$$

where $\kappa,\ q \in \mathbb{R}$ are constants defining the slope and intercept of the function $a(k)$ within its domain, as Fig. 3 depicts. An analysis of the effect of the parameter values on the disconnection dynamics is in Appendix A.

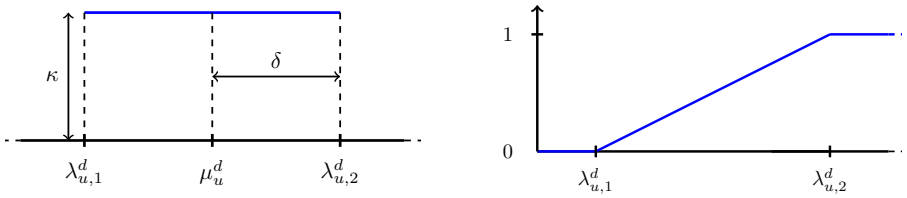

(a) Probability distribution function of p_u^d. κ represents the height, δ represents the half-width of the domain Λ_u^d.

(b) Cumulative distribution function of p_u^d. κ represents the slope of the linear function confined within the domain Λ_u^d.

Fig. 3: Probability (left) and cumulative (right) distribution function of p_u^d, the under-frequency disconnection scenario.

2.2 Frequency Dynamics and Feedback Model with Solar Energy

We briefly present the electricity grid model, derived from [24], as a second-order transfer function, $G(z, R)$, which depends on the amount of renewable power R feeding the network. We denote the total load of the network as S: notice that $R \leq S$, where $S = R$ holds in a network solely based on renewable energy sources. The presence of renewables injecting power in the grid modifies its inertia [25]: as discussed in [6], in this work we assume a linear relationship between the amount of renewables in the grid and its inertia, which will appear in the model parameters α_1 and α_2.

$G(z, R)$ relates the solar power deviation, $\Delta P_{PV}(k)$ (its input) to the frequency deviation $\Delta f(k)$ (output) as

$$\Delta f(k) = G(z, R)[P_{PV}(k) - P_{PV,0}], \tag{2}$$

where $\Delta f = f - f_0$, $\Delta P_{PV} = P_{PV} - P_{PV,0}$, and $P_{PV,0}$ represents the initial power produced by the solar panels. $G(z, R)$ can be written as

$$G(z, R) = \frac{\beta_1 z + \beta_2}{z^2 + \alpha_1(R) z + \alpha_2(R)}.$$

Here $\alpha_1(R)$, $\alpha_2(R)$, β_1, β_2 are parameters that are selected to render the transfer function stable; in particular $\alpha_1(R)$ and $\alpha_2(R)$ linearly depend the amount of renewable power in the network, as mentioned above.

Remark 1. The total power output of the solar population $P_{PV}(k)$ is proportional to the portion of panels in the ON mode ($x(k)$), as $P_{PV}(k) \sim \bar{P}Nx(k)$, where $\bar{P}$ is assumed to be the deterministic power output of a single PV panel, and N represents the total number of panels. The unpredictability of weather conditions will be modelled as an additional noise. This relationship links the network model in Eqn. (2) with the solar devices dynamics in Eqn. (1). □

We couple in a feedback fashion the transfer function of the electric network in Eqn. (2), expressed as a difference equation in the first line below, with the (time-varying) Markov chain modelling the solar panels dynamics in Eqn. (1), as:

$$\begin{cases} \Delta f(k+1) = \alpha_1 \Delta f(k) + \alpha_2 \Delta f(k-1) + \beta_1 \Delta P_{PV}(k) + \beta_2 \Delta P_{PV}(k-1) + \omega_f(k) \\ x(k+1) = (1 - a(k))x(k) + b(k)\varepsilon(k)y(k) \\ y(k+1) = b(k)(1 - x(k) - \varepsilon(k)y(k)), \end{cases} \tag{3}$$

where

$$P_{PV}(k) = \bar{P}Nx(k) + \omega_P(k).$$

Note, unlike Eqn. (2), the addition of the noise terms $\omega_f \in \mathcal{N}(0, \sigma_f)$ and $\omega_P \in \mathcal{N}(0, \sigma_P)$. These quantities represent respectively the power unbalances between generation and load that naturally occur in the electric network, and the unpredictability of solar panels (their power output depends on characteristics as weather conditions, occlusions, temperature). The term $P_{PV}(k)$ represents the solar power injected in the grid at time k, and $\Delta P_{PV}(k) = P_{PV}(k) - P_{PV,0}$, where $P_{PV,0}$ is the value at the equilibrium. The dynamics of $\Delta P_{PV}(k+1)$ can be computed substituting $P_{PV}(k) = \Delta P_{PV}(k) + P_{PV,0}$. Noise processes $\omega_f(k)$ and $\omega_P(k)$, are made up by i.i.d. random variables, characterised by density functions $t_f(\cdot)$ and $t_P(\cdot)$. $\omega_f(\cdot)$ and $\omega_P(\cdot)$ are independent of each other. Notice that variables x and y evolve deterministically, however they represent expected values for the temporal evolution of a Markov chain, and as such do not require additional noise terms.

3 Formal Abstractions and Parameter Synthesis

In this section we generate a finite abstraction of the system in Eqn. (3), which results in a dtMC, and later perform parametric model checking on the dtMC.

We first rename the variables delayed by one-step (i.e. $\Delta f(k-1)$ and $\Delta P_{PV}(k-1)$) in order to obtain state variables that are coherent in time. We therefore introduce two new state variables:

$$\phi(k) = f(k-1), \quad \text{s.t. } \Delta\phi(k) = f(k-1) - f_0 = \Delta f(k-1),$$

$$\xi(k) = P_{PV}(k-1), \quad \text{s.t. } \Delta\xi(k) = P_{PV}(k-1) - P_{PV,0} = \Delta P_{PV}(k-1).$$

The model described in Eqn. (3) becomes

$$\begin{cases} \Delta f(k+1) = \alpha_1 \Delta f(k) + \alpha_2 \Delta\phi(k) + \beta_1 \Delta P_{PV}(k) + \beta_2 \Delta\xi(k) + \omega_f(k) \\ \Delta\phi(k+1) = \Delta f(k) \\ x(k+1) = (1 - a(k))x(k) + b(k)\varepsilon(k)y(k) \\ y(k+1) = b(k)(1 - x(k) - \varepsilon(k)y(k)) \\ P_{PV}(k) = \bar{P}Nx(k) + \omega_P(k) \\ \xi(k+1) = P_{PV}(k). \end{cases} \tag{4}$$

The state-space $\mathcal{Q}$ is thus composed of six continuous variables: $x(k)$ and $y(k)$ belong to the interval $\mathbb{X} = [0, 1]$; $\Delta f(k)$, $\Delta\phi(k)$ belong to $\mathbb{F} = [f_u, f_o] = [-0.8, +0.8]$ Hz, corresponding to network frequency in $[49.2, 50.8]$ Hz (our modeling framework is valid for values $f \simeq f_0$); $P_{PV}(k)$ and $\xi(k)$ range within $\mathbb{P} = [0, \bar{P}N]$, i.e. between zero and the max power resulting from the sum of individual contributions. Define the global state vector as $q = (\Delta f, \Delta\phi, x, y, P_{PV}, \xi) \in \mathbb{F}^2 \times \mathbb{X}^2 \times \mathbb{P}^2 = \mathcal{Q}$ and introduce the noise vector $\omega = (\omega_f,\ \omega_P)$.

The noise term $\omega(k)$ defines the transition probabilities of the discrete-space Markov model in the formal abstraction procedure, as explained shortly. Consider the equation $P_{PV}(k+1) = \bar{P}Nx(k) + \omega_P(k)$ from the system of equations in (4). The deterministic term $\bar{P}Nx(k)$ can be seen as the (time-varying) average value of noise $\omega_P(k) \in \mathcal{N}(0, \sigma_P)$, i.e. $P_{PV}(k+1) \in \mathcal{N}(\bar{P}Nx(k), \sigma_P)$. Thus, transitions between states q and q' are determined [15] via $t_\omega(\cdot|q) = (t_f(\cdot|q), t_P(\cdot|q))$, the one-step transition density function of $\omega(k)$ conditional on point q, where $t_f(\cdot|q)$, $t_P(\cdot|q)$ are the transition density of ω_f and ω_P conditional on point q, respectively. The two densities t_f and t_P are decoupled, in view of the assumed independence of the two noise processes.

3.1 Finite Abstractions via State-Space Partitioning

We now tailor to our setup a formal abstraction technique, first proposed in [15], which is aimed at reducing a discrete-time, uncountable state-space Markov process into a discrete-time, finite-state Markov chain $\mathcal{M}$. The abstraction is based on a state-space partitioning procedure.

To ease notation and understanding, consider a simpler system made of just two variables x_1 and x_2, belonging to intervals $[l_1, u_1]$ and $[l_2, u_2]$ respectively, and define the state vector $q = (x_1, x_2)$ within domain $\mathcal{Q}$. Choose ν_x, a discretisation step for both variables (for simplicity we use the same step, whilst in principle we could select two different ν_1, ν_2 for x_1 and x_2, respectively), such that $u_1 - l_1 = N_1\nu_x$ and $u_2 - l_2 = N_2\nu_x$. In other words, divide intervals $[l_1, u_1]$ and $[l_2, u_2]$ into N_1 and N_2 subintervals, so to obtain a $(N_1 \times N_2)$-rectangle grid. Denote each rectangle as q_i, $i = 1, \dots N_1 \cdot N_2$. Fig. 4 displays an example of a state-space partitioning procedure, where $N_1 = 3$ and $N_2 = 2$, and the associated computation of the abstracted Markov model. Each of the q_i rectangles is mapped into an abstract state s_i of a $(N_1 \times N_2)$-state Markov model.

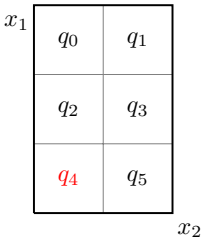

(a) State-space partitioning: each rectangle is mapped into a dtMC state (region q_4 marked *unsafe*).

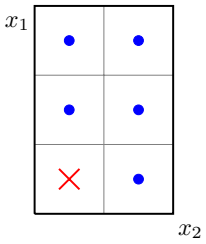

(b) Reference points of the grid. State s_4 is indicated with a cross for visualisation purposes.

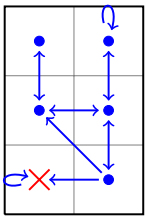

(c) Transition probabilities are computed as the marginalised integral of the kernel of the noise signal.

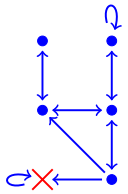

(d) Resulting dtMC: abstract states as partition of state space, transitions as integral of noise signal.

Fig. 4: Construction of the Markov chain from a two-dimensional continuous-state model, with $N_1 = 3$ and $N_2 = 2$.

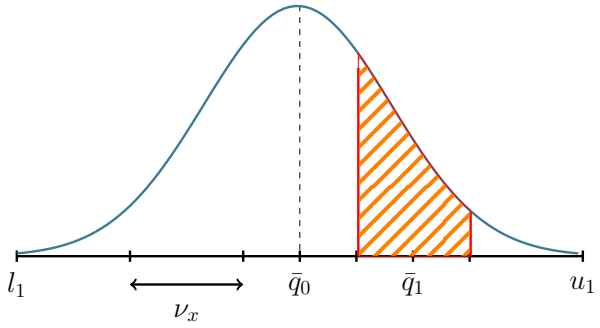

Fig. 5: Computation of the transition probability $P(s_0, s_1)$ in a one-dimensional system: imagine variable $x \in [l, u]$ partitioned into intervals q_i, with reference points $\bar{q}_i$. Each interval q_i is mapped into the abstract state s_i. The transition kernel density is centred at $\bar{q}_0$, the reference point of q_0, thus $P(s_0, s_1)$ is the integral of such kernel density over q_1 (region corresponding to s_1). In a two-dimensional system the integral is computed over a rectangle, whereas in higher dimensions over a hyper-rectangle.

Notice that in Fig. 4 we have introduced a "label" for state q_4: *unsafe*. (Parametric) model checking employs labels to define specifications as objectives of verification. In particular, parameter synthesis aims at minimising the reachability probability of q_4. Conversely, states q_i, $i \neq 4$, are deemed *safe*, representing ordinary operating conditions for the model. Subsequently we'll refer to states of the models as *safe* or *unsafe*. Whilst in this work we limit ourselves to the study of safety/reachability properties, evidently in formal verification much more complex specifications are allowed.

The transition probabilities among the generated abstract states are computed as follows. Choose an arbitrary reference point $\bar{q}_i$ within each rectangle q_i, e.g. its centre. This represents the point from which transition probabilities are computed. Consider, as an example, the transition from region q_0 to region q_1, that is, from state s_0 to state s_1. Imagine to centre the noise kernel over point $\bar{q}_0$, as per Fig. 5. The transition probability between q_0 and q_1 is obtained as the integral of the density of the noise kernel, centred at $\bar{q}_0$, over region q_1 (the area corresponding to s_1).

Considering now the six-dimensional system in Eqn. (4), recall that each variable belongs to the finite interval $[l_i, u_i]$, $i = 1, \dots 6$. Choose ν_i, a discretisation step for the six variables, such that $u_i - l_i = N_i \nu_i$. In other words, divide intervals $[l_i, u_i]$ into N_i subintervals, $i = 1, \dots 6$, so to obtain a N_P-dimensional hyper-rectangle grid, where $N_P = \prod_1^6 N_i$. Index the hyper-rectangles $q_r = (\Delta f_r, \Delta\phi_r, x_r, y_r, \Delta P_{PV,r}, \Delta\xi_r)$, $r = 1, \dots N_P$. Define $\bar{q}_r$ as the reference point of the hyper-rectangle q_r, e.g. its centre of mass. We therefore compute $P(s, s')$, the transition probability from state s to state s', corresponding to the transition from region q to region q', as

$$P(s, s') = \int_{q'} t_\omega(u|\bar{q})du \ . \tag{5}$$

For reasons related to details of model checking algorithms (cf. below), whenever a state is deemed unsafe (denoted as s_U), it is made absorbing (namely with a self-loop probability equal to one). The verification goal of interest is safety computation, namely the computation of the probability of remaining within a safe region of the state-space: whenever the system enters the unsafe set, the safety property is violated ever after (this corresponds to the impossibility of leaving such set, as set above). The abstract Markov chain $\mathcal{M}$ is thus composed of states s whose transitions are defined as per Eqn. (5).

The abstraction procedure applied to the model in (4) carries a discretisation error: in the next section bounds for this error are calculated as a function of the discretisation steps ν_f (for frequency-related variables) and ν_P (for power-related variables). As argued in [15], a finer grid is expected to result in a smaller abstraction error, however it generates a larger abstract finite state space.

3.2 Load-shedding as the Complement of a Safety Property

In this section we formally characterise load-shedding as the complement of a safety property. Qualitatively, a safety property asserts that *nothing unsafe*

happens during the dynamical evolution of a model. Deeming *unsafe* a load-shedding scenario, the absence of load-shedding corresponds to a safety property for the model in (4). As such, we compute the opposite, namely the probability of an *unsafe condition* happening, as the complement of a safety property (the earlier is also technically known as a reachability property [26]).

Consider the model in (4) with initial state q_0 and select a discrete-time horizon H. We assume the electric network activates the load-shedding procedure whenever $f(k) \leq 49.2$ Hz. Define the load-shedding set as $\mathcal{L} := \{q = (\Delta f_r, \Delta\phi_r, x_r, y_r, \Delta P_{PV,r}, \Delta\xi_r) \mid \Delta f_r \leq -0.8 \text{ Hz}\}$. The aim of the verification procedure is the computation of the reachability probability of states $q \in \mathcal{L}$, formally

$$p_{q_0}(\mathcal{L}) := \text{Prob}\{q(i) \in \mathcal{L}, i \in [1, H] \mid q_0\}. \tag{6}$$

This reachability probability can be formally characterised via value functions $V_k : \mathcal{Q} \to [0, 1]$, $k = 1, \dots H$, which can be computed recursively as [26]

$$V_k(q) = \mathbf{1}_{\mathcal{L}}(q) \int_{\mathcal{Q}} V_{k+1}(u) t_\omega(u|q) du, \quad \text{with } V_H(q) = \mathbf{1}_{\mathcal{L}}(q), \tag{7}$$

so the initial value function $V_1(q_0) = p_{q_0}(\mathcal{L})$ is the quantity of interest. We utilise a procedure presented in [26] to approximate the model in Eqn. (4). We therefore define the discrete version of Eqn. (6), as

$$p_{s_0}(\mathcal{L}_s) := \text{Prob}(s(i) \in \mathcal{L}_s, i \in [1, H] \mid s_0) = V_1^s(s_0),$$

where $\mathcal{L}_s := \{\bar{f} \in \mathcal{F}_0\}$ (consider it the dtMC-equivalent of $\mathcal{L}$), $V_1^s(\cdot)$ is the value function computed over $\mathcal{S}$ similarly to Eqn. (7), and s_0 represents the initial state of the dtMC according to the procedure in Section 3.1.

If we now abstract the aggregated population of solar panels as a Markov chain based on the procedure of Section 3, and compute the solution of Eqn. (7) over the Markov chain $p_{s_0}(\mathcal{L}_s)$, then the overall approximation error can be upper-bounded [26] as follows

$$|p_{q_0}(\mathcal{L}) - p_{s_0}(\mathcal{L}_s)| \leq (H - 1) \left[\eta_1 \frac{\nu_f}{\sigma_f} + \eta_2 \frac{\nu_P}{\sigma_P}\right],$$

where η_1, η_2 are constants (see [17]) obtained from the dynamics in Eqn. (4). This error allows to translate the outcomes of the verification procedure (obtained from the Markov model) over the concrete population model, and in particular to compute the unknown quantity $p_{q_0}(\mathcal{L})$. As mentioned above, ν_f and ν_P can be tuned to reduce the abstraction error to a desired precision [26].

3.3 Parameter Synthesis: Guaranteeing Model Safety

Whilst the verification procedure describe in the previous section aims at checking a property against a given concrete (non-parameterised) model, the parameter synthesis problem studies which parameter values correspond to models that verify the considered property. For a set Θ of n parameters $\theta_1, ..., \theta_n$, we define a parametric dtMC as follows:

Definition 2 (p-dtMC). *A parametric dtMC over the set Θ of parameters is a tuple $D(\Theta) = (\mathcal{S}, s_0, P[\Theta])$, where $\mathcal{S}$ and s_0 are as before, and $P[\Theta] : \mathcal{S} \times \mathcal{S} \to [0, 1]$ is the parametric probability transition matrix.*

Definition 3 (Instance dtMC). *For p-dtMC(Θ) and valuation $\bar{\theta}$, $D^{(\Theta)}[\bar{\theta}]$ (or simply $D[\bar{\theta}]$) is the instance dtMC of D(Θ) obtained by instantiating $\theta_i \in \Theta$ with $\bar{\theta}(\theta_i)$.*

The formal abstraction technique described above defines a Markov chain $\mathcal{M}[\theta]$ depending on $\theta = (\mu_i^j, \varsigma_i^j, S, R)$, where μ_i^j and ς_i^j are the mean and variance of p_i^j, $i \in \{u, o\}$, $j \in \{d, r\}$, and S and R are the total load the network and penetration of renewable sources, respectively (recall that $R \leq S$).

We define the synthesis region Θ_s as the set of instantiations, such that each instance (or point) $\theta = (\theta_1, ..., \theta_n)$ induces an instance p-dtMC$[\theta]$, for which the safety property is satisfied. The aim is to find (at least an approximation of) the synthesis region Θ_s. Notice that in general it is non-trivial to get the exact shape of such a parametric region. As a consequence, we introduce a discretisation of the parameter space and exhaustively search the satisfying parameter values over the discretisation.

Define the range of parameters as Θ_{range}. Given the parameter set Θ and its range Θ_{range}, we specify a discretization step $\delta_i \in \mathbb{R} > 0$ for each parameter $\theta_i, (i = 1, \dots n)$, such that $u_i^\theta - l_i^\theta = Q_i \delta_i$, where the interval $[l_i^\theta, u_i^\theta]$ represents the range of values that parameters θ_i can take. Namely, the range $[l_i^\theta, u_i^\theta]$ is divided into Q_i intervals, thus partitioning Θ_{range} into a grid of $\prod_{i=1}^{n} Q_i$ hyper-rectangles. We define for each of these hyper-rectangles a reference point $\bar{\theta}^{(i)} = (\bar{\theta}_1, ..., \bar{\theta}_n)$ that induces an instance dtMC$[\bar{\theta}^{(i)}]$: notice that this implicitly means that instead of checking each point of the (continuous) region Θ_{range}, we exclusively evaluate the sample points $\bar{\theta}^{(i)}$.

Interestingly, there is no linear mapping between any of the parameters in $\theta = (\mu_i^j, \varsigma_i^j, S, R)$ and the transition probability matrix P: varying such parameters causes a shifting of the elements $P(s, s')$ rather than linearly influencing them, as the following example shows.

Example 1. Recall the system in Eqn. (4), and consider, for simplicity, solely

$$x(k+1) = (1 - a(k)) \cdot x(k) + b(k)\varepsilon(k)y(k),$$

in an under-frequency scenario. Let us analyse the effect of the distribution variance ς_u^d. Focus on the $(1 - a(k))$ term: it is a function of $f(k)$, precisely of the deviation of $f(k)$ from f_0, as $a(k) = \int_{f(k)}^{+\infty} p_u^d(u)du$. Imagine the abstraction procedure to be coarse such that Λ_u^d, the domain of p_u^d, is divided into three intervals. According to this partitioning choice, the value of ς_u^d and the value of the frequency $f(k)$, the transition ON-to-OFF can take three values, as shown in Fig. 6: values being $(0, 0.5, 1)$ or $(0.25, 0.5, 0.75)$. Increasing the variance "spreads" the values of $a(k)$ within the partition intervals. Considering the mean value of p_u^d, the domain Λ_u^d shifts closer or away from f_0 when the mean is increased or decreased. Varying parameters θ_i changes in a non-linear way (the function is indeed an integral) the transition probabilities. □

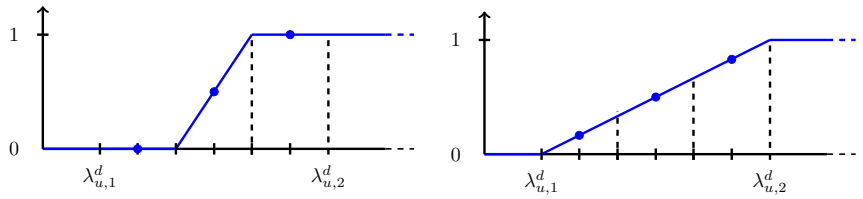

(a) $a(k)$ with small variance. (b) $a(k)$ with high variance.

Fig. 6: If p^d_u is modeled with a small variance (left), transition probability assume values $(0, 0.5, 1)$, whereas a high variance (right) leads to $(0.25, 0.5, 0.75)$.

4 Case Study: Reliability Analysis for the Grid Dynamics in the Presence of Solar Energy Sources

In this section we translate the theory presented above and present results on a reliability study for the model of the electric network with PV generation, under different scenarios. We synthesise parameters $\theta = (\mu^j_i, \varsigma^j_i, S, R)$, $i \in \{u, o\}$, $j \in \{d, r\}$, using the Markov model resulting from the procedure illustrated in Section 3.

Following the ENTSO-E guidance [24], we have tested an in-feed loss of 3 GW in global networks with respectively low demand ($S = 220$ GW) and high demand ($S = 440$ GW) scenarios. The network model parameters in Eqn. (2) are selected according to [24]. Power and frequency values are normalised (per unit) relative to S and to 50 Hz. Power production of a single panel $\bar{P}$ is set to 3 kW. The variance σ_P is set to 1% of $\bar{P}$. The variance σ_f is set to 0.05. Time delays are modelled in accordance with [7, 8]: the minimum reconnection delay is set to 20 seconds, the maximum to 40 seconds.

Parameter synthesis tests are implemented using MATLAB software. Given the size of the state space, the discretisation steps ν_f (for frequency-related variables) and ν_P (for power-related variables) are set to 0.01 and 0.05 respectively. The grid frequency is sampled at a rate of 0.2 s, consistently with the requirements introduced in [27]. The analysis is focused on a few seconds following an incident: simulation time is set to 20 s. After this time interval, we reasonably assume that the primary and secondary network control would kick in and would stabilise the signal $f(\cdot)$ around its nominal value. The discrete time horizon is thus composed of 100 steps: results of every scenario in the following section carry an abstraction error of 0.1, as per Section 3.2. Parameters θ are synthesised satisfying a maximum load-shedding probability formula, as $p_{s_0}(\mathcal{L}_s) \leq \zeta$, where $\zeta = 0.1$: if θ satisfies this property, we include it in Θ_s.

4.1 Injection of Faults as Generation Losses

As anticipated above, Transmission Systems Operators are tasked with ensuring the safe operation of the grid, and are thus interested in formal guarantees on

its dynamics, and in reliable forecasting of potentially problematic situations, such as issues related to frequency responses after a generation loss incident. Renewables, and solar power in particular, reduce the total inertia of the power network: this results in a network that is more prone to oscillations [5], and thus to possibly higher frequency deviations.

We assume the initial condition to be $f(0) = f_0$, with the population of panels in active (ON) mode ($x(0) = 1$). A generation-loss incident is modelled as a negative step injected into the power dynamics. Assuming that an incident of magnitude M occurs at time $k = \bar{k}$, the dynamics of $f(\bar{k}+1)$ become

$$\Delta f(\bar{k}+1) = \alpha_1 \Delta f(\bar{k}) + \alpha_2 \Delta\phi(\bar{k}) + \beta_1(\Delta P_{PV}(\bar{k}) - M) + \beta_2 \Delta\xi(\bar{k}) + \omega_f(\bar{k}), \quad (8)$$

and then evolve at time $(\bar{k}+2)$ as

$$\begin{aligned}\Delta f(\bar{k}+2) = \alpha_1 \Delta f(\bar{k}+1) + \alpha_2 \Delta\phi(\bar{k}+1) + \beta_1(\Delta P_{PV}(\bar{k}+1) - M) + \\ + \beta_2(\Delta\xi(\bar{k}+1) - M) + \omega_f(\bar{k}+1).\end{aligned} \quad (9)$$

Equations (8) and (9) display two different deterministic drifts. Their abstraction by discretisation leads to two different abstract Markov chains $\mathcal{M}_1$ and $\mathcal{M}_2$, with different transition matrices P_1 and P_2 but with the same state space. In our tests we consider that $\bar{k} = 0$, namely we assume that the incident occurs at the beginning of the time horizon when all quantities are at rest. This setup results in a time-varying safety verification problem: given the initial probability distribution vector π_0, the dynamics evolve as

$$\pi_1 = \pi_0 \cdot P_1, \qquad \pi_H = \pi_1 \cdot (P_2)^{H-1},$$

where π_H is a vector with the probabilities of being in each state after H steps.

4.2 Outcomes of the Parameter Synthesis Problem and Analysis

Our tests encompass several industrially relevant scenarios, in which we vary: (1) the mean and variance of p_i^j, $i \in \{u, o\}$, $j \in \{d, r\}$; (2) the total solar penetration in the network R; and (3) the total load of the network S. Recall from Eqn. (2) that solar penetration modifies the network transfer function. The considered ranges for the parameters are summarised in Table 2. Solar penetration accounts for 10% – 40% of the network load, which well represents current values for solar power contribution (e.g. Germany's 2017 average production is around 7%, reaching peaks of 60% in Summer [2]). In this work we consider a single, heterogeneous population, namely every solar device belongs to a given p_i^j distribution. We might consider two (or more) populations, each with diverse parameters: Appendix B discusses two modelling approaches to encompass this.

The threshold distributions for $\mathcal{I}_f$ are uniform, as discussed in Section 2.1: the mean value μ_i^j ideally represents specific regulations on disconnection and reconnection, whereas the variance ς_i^j represents small manufacturing deviations from the desired value. Finally, increasing variance of p^d and p^r reflects a more heterogeneous population (in terms of $\mathcal{I}_f$ thresholds).

Load Demand [GW]	Renewable [% S]	μ_u^d [Hz] (step: 0.05)	ς_u^d [Hz^2] (step: 0.25)
220, 440	10, 20, 30, 40	$[49.5, 49.8]$	$[1, 7.5] \cdot 10^{-3}$

Table 2: Parameters range over set Θ_{range}

Renewables	μ_u^d [Hz]						
R [% S]	49.5	49.55	49.6	49.65	49.7	49.75	49.8
10	sat	sat	6	2.5	–	–	–
20	sat	sat	4.5	1.5	–	–	–
30	sat	sat	2.5	–	–	–	–
40	sat	4.5	–	–	–	–	–

Table 3: Boundaries of synthesis region Θ_s with $S = 220$ GW. The table shows the highest value of ς_u^d that satisfies the property; entries `sat` and $-$ indicate that all values and no values, respectively, satisfy the property.

Figures 7 and 8 depict the load-shedding probability in the presence of 20% solar penetration, with a network load $S = 220$ GW and $S = 440$ GW, respectively, where values of μ_u^d range within $[49.5, 49.8]$ Hz and those of ς_u^d are within $[1, 7.5]$ Hz^2. A higher ς_u^d causes a higher number of panels to have disconnection thresholds closer to f_0, as per Fig. 6 in Section 3.3. Consequently, a greater portion of the population is likely to disconnect under frequency deviations, causing the network frequency to decrease. As intuitive, parameter S plays a major role in the outcome of the verification. Table 3 shows the "boundary points" of Θ_s, namely the largest values of ς_u^d for each μ_u^d that satisfy the property. In a low demand setting ($S = 220$ GW), the load-shedding probability is essentially binary (values close to zero or to one), whereas in a high demand scenario ($S = 440$ GW) the load-shedding probability grows smoothly with μ_u^d and ς_u^d, never reaching the critical value ζ (thus for $S = 440$ GW, $\Theta_{range} = \Theta_s$). A high-demand network is thus more resilient to incidents, since it has a greater inertia, and an incident has proportionally less impact: the maximum load-shedding probability value is around 1.5%. The tests with a wider penetration of solar contributions (10%, 30%, 40% of the total), as shown in Fig. 9, indicate that the load-shedding probability increases when a larger population is connected to the grid: this is intuitive, as more renewable energy renders the frequency response more oscillatory, and thus more likely to deviate from f_0.

The abstraction procedure introduced in Section 3 carries an error of 0.1 with the tested ν_f and ν_P. Parameters in θ are synthesised accounting for a maximum load-shedding probability (in the abstract Markov model) of $\zeta = 0.1$. As such, using parameters within the set Θ_s, the load-shedding probability on the concrete model (as in Eqn. (3)) results to be $p_{q_0}(\mathcal{L}) \leq 0.2$. As discussed, a refinement of ν_f and ν_P allows reducing the error between the real and abstract systems to match any desired precision [26].

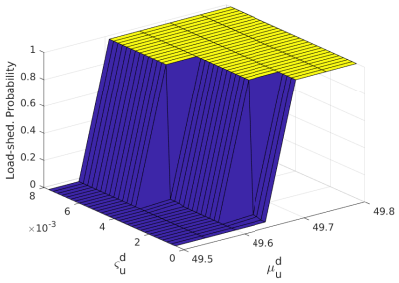

Fig. 7: Load-shedding probability with $S = 220$ GW, $R = 0.2S$, μ_u^d and ς_u^d as per Table 2.

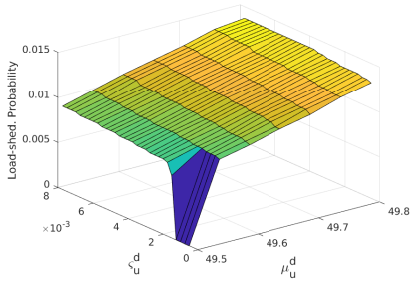

Fig. 8: Load-shedding probability with $S = 440$ GW, $R = 0.2S$, μ_u^d and ς_u^d as per Table 2.

5 Conclusions and Future Work

In this work we have developed a formal approach to synthesise model parameters, which represent the heterogeneity of a population of solar panels connected to the electricity grid: this parameter synthesis yields models that verify a property of interest. We have presented a formal parameter synthesis study of grid reliability under significant energy generation from renewables. The focus of the verification procedure has been on a safety property, describing the requirement that the network frequency remains within given bounds over a finite time horizon (absence of a load-shedding scenario) under a power generation loss. Transmission Systems Operators can employ the presented technique to monitor the distribution and characteristics of solar panels over the grid, and to assess its reliability in the case of incidents.

Future work includes extensions to several populations of solar devices, using different distribution of disconnection/reconnection thresholds, and modelling the solar output as a stochastic equation depending on weather forecast.

References

1. ENTSO-E: Statistical factsheet. Tech. rep. (2016)
2. H. Wirth: Recent Facts about Photovoltaics in Germany. Tech. rep., Fraunhofer ISE (2018)
3. Solar Power Europe: Global Market Outlook for Solar Power 2016-2020. Tech. rep. (2016)
4. Peruffo, A., Guiu, E., Panciatici, P., Abate, A.: Aggregated Markov Models of a Heterogeneous Population of Photovoltaic Panels. International Conference on Quantitative Evaluation of Systems pp. 72–87 (2017)
5. Peruffo, A., Guiu, E., Panciatici, P., Abate, A.: Impact of Solar Panels and Cooling Devices on Frequency Control after a Generation Loss Incident. In: Decision and Control (CDC) 2018 IEEE 57th Annual Conference Proceedings. IEEE (2018)
6. Peruffo, A., Guiu, E., Panciatici, P., Abate, A.: Synchronous Frequency Grid Dynamics in the Presence of a Large-Scale Population of Photovoltaic Panels. In: 2018 Power Systems Computation Conference (PSCC). pp. 1–7 (June 2018)

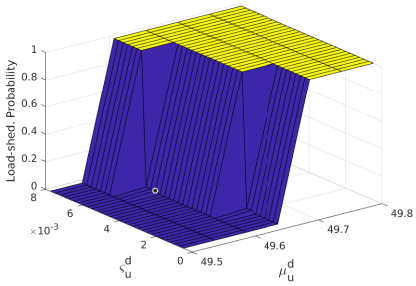

(a) 10% solar penetration with network load $S = 220$ GW.

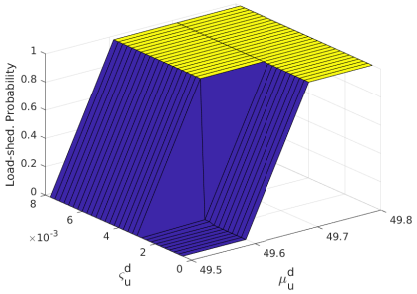

(b) 30% solar penetration with network load $S = 220$ GW.

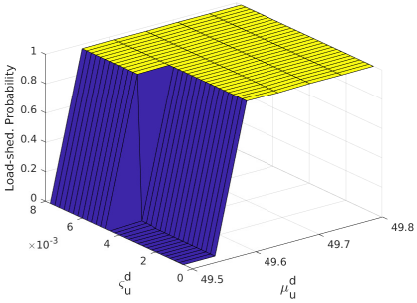

(c) 40% solar penetration with network load $S = 220$ GW.

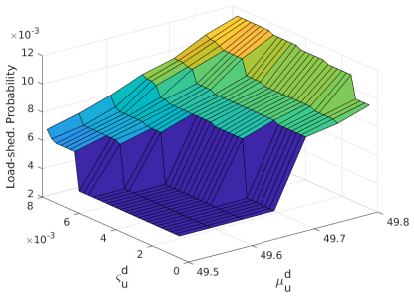

(d) 10% solar penetration with network load $S = 440$ GW.

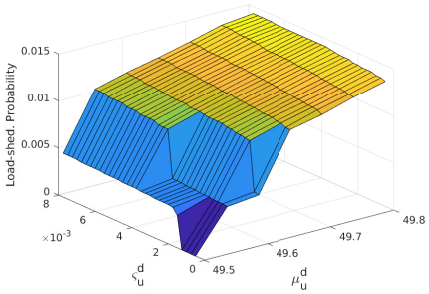

(e) 30% solar penetration with network load $S = 440$ GW.

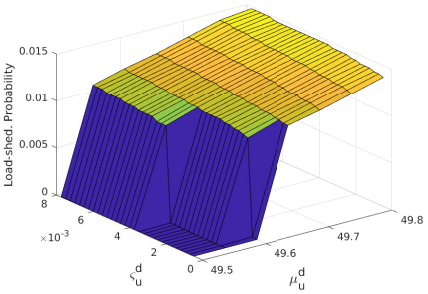

(f) 40% solar penetration with network load $S = 440$ GW.

Fig. 9: Load-shedding probability with parameter ranges $\mu_u^d \in [49.5, 49.8]$ Hz, $\varsigma_u^d \in [1, 7.5] \cdot 10^{-3}$ Hz^2.

7. M. Jung, O. Wiss, B.L.: Analyses et conclusions – Tests en sous-frequence. Tech. rep., RTE (2016)
8. M. Jung, O. Wiss, B.L.: Analyses et conclusions – Tests en sur-frequence. Tech. rep., RTE (2016)
9. Moslehi, K., Kumar, R., et al.: A reliability perspective of the smart grid. IEEE Trans. Smart Grid 1(1), 57–64 (2010)
10. Zhang, P., Wang, Y., Xiao, W., Li, W.: Reliability evaluation of grid-connected photovoltaic power systems. IEEE transactions on sustainable energy 3(3), 379–389 (2012)
11. Albasrawi, M.N., Jarus, N., Joshi, K.A., Sarvestani, S.S.: Analysis of reliability and resilience for smart grids. In: 2014 IEEE 38th Annual Computer Software and Applications Conference. pp. 529–534. IEEE (2014)
12. Alagoz, B., Kaygusuz, A., Karabiber, A.: A user-mode distributed energy management architecture for smart grid applications. Energy 44(1), 167–177 (2012)
13. Volkanovski, A., Čepin, M., Mavko, B.: Application of the fault tree analysis for assessment of power system reliability. Reliability Engineering & System Safety 94(6), 1116–1127 (2009)
14. Hartmanns, A., Hermanns, H.: Modelling and Decentralised Runtime Control of Self-stabilising Power Micro Grids. In: International Symposium On Leveraging Applications of Formal Methods, Verification and Validation. pp. 420–439. Springer (2012)
15. Abate, A., Soudjani, S.E.Z.: Quantitative Approximation of the Probability Distribution of a Markov Process by Formal Abstractions. Logical Methods in Computer Science 11 (2015)
16. Soudjani, S.E.Z., Gerwinn, S., Ellen, C., Fränzle, M., Abate, A.: Formal Synthesis and Validation of Inhomogeneous Thermostatically Controlled Loads. In: International Conference on Quantitative Evaluation of Systems. pp. 57–73 (2014)
17. Soudjani, S.E.Z., Abate, A.: Aggregation and Control of Populations of Thermostatically Controlled Loads by Formal Abstractions. IEEE Transactions on Control Systems Technology 23(3), 975–990 (2015)
18. Han, T., Katoen, J.P., Mereacre, A.: Approximate parameter synthesis for probabilistic time-bounded reachability. In: 2008 Real-Time Systems Symposium. pp. 173–182. IEEE (2008)
19. Daws, C.: Symbolic and parametric model checking of discrete-time markov chains. In: International Colloquium on Theoretical Aspects of Computing. pp. 280–294. Springer (2004)
20. PRISM website. https://www.prismmodelchecker.org/
21. MODEST website. http://www.modestchecker.net/
22. Soudjani, S.E.Z., Gevaerts, C., Abate, A.: FAUST^2: Formal Abstractions of Uncountable-STate STochastic Processes. In: International Conference on Tools and Algorithms for the Construction and Analysis of Systems. pp. 272–286. Springer (2015)
23. Cauchi, N., Abate, A.: StocHy: Automated verification and synthesis of stochastic processes. In: International Conference on Tools and Algorithms for the Construction and Analysis of Systems. pp. 247–264. Springer (2019)
24. ENTSO-E: Policy 1: Load-frequency Control and Performance. Tech. rep. (2009)
25. Tielens, P., Van Hertem, D.: Grid inertia and frequency control in power systems with high penetration of renewables. In: Young Researchers Symposium in Electrical Power Engineering. vol. 93, p. 101 (2012)
26. Abate, A., Katoen, J.P., Lygeros, J., Prandini, M.: Approximate model checking of stochastic hybrid systems. European Journal of Control 16(6), 624–641 (2010)

27. European Commission: Commission regulation (EU) 2016/631 of 14th april 2016. Tech. rep. (2016)

A Analysis of the Effect of Parameters on Stability

In this section we study the effect of parameters μ_i^j and ς_i^j (strictly related to constants κ, q), on the Markov chain model and on the associated probability of load shedding. As previously stated, our interest lies on a generation-loss incident scenario. The worst-case analysis is carried out considering the following situation: the whole solar population is at risk of disconnection when the incident occurs. We therefore envision that at time k, all panels are ON, i.e. $x(k) = 1$ and $y(k) = 0$. Noting that $\kappa f(k) + q \leq 1 \; \forall k$, the model in Equation (3) assumes three separate modes as

$$\begin{cases} f(k+1) = \alpha_1 f(k) + \alpha_2 f(k-1) \beta_1 x(k) + \beta_2 x(k-1) \\ x(k+1) = \begin{cases} x(k) & f(k) > \lambda_{u,2}^d \\ (1 - \kappa f(k) - q) x(k) & f(k) \in \Lambda_u^d \\ 0 & f(k) < \lambda_{u,1}^d. \end{cases} \end{cases} \tag{10}$$

Substitute $\phi(k) = f(k) - f_0$ and $\chi(k) = x(k) - x_0$, and compute the equilibrium points (denoted $\overline{\phi}, \overline{\chi}$) as

$$\overline{\phi} = \frac{\beta_1 + \beta_2}{1 - \alpha_1 - \alpha_2} \cdot \overline{\chi}, \qquad \overline{\chi} = \begin{cases} \overline{\chi} = \overline{\chi} & f(k) > \lambda_{u,2}^d \\ c_1 \overline{\chi}^2 + c_2 \overline{\chi} + c_3 & f(k) \in \Lambda_u^d \\ \overline{\chi} = -x_0 & f(k) < \lambda_{u,1}^d, \end{cases}$$

where

$$c_1 = -\kappa \frac{\beta_1 + \beta_2}{1 - \alpha_1 - \alpha_2}, \quad c_2 = -q - \kappa x_0 \frac{\beta_1 + \beta_2}{1 - \alpha_1 - \alpha_2}, \quad c_3 = -q x_0.$$

Rewrite κ and q as a function of μ_u^d and δ_u^d (cf. Fig. 3) as

$$\kappa = -\frac{1}{2\delta_u^d}, \quad q = \frac{1}{2\delta_u^d}(\mu_u^d + \delta_u^d).$$

Note that κ is negative because we consider the under-frequency scenario, i.e. $\lambda_{u,1}^d < \mu_u^d < \lambda_{u,2}^d$. Substitute κ and q, so the equilibrium point for $f(k) \in \Lambda_u^d$ becomes

$$\frac{\beta_1 + \beta_2}{1 - \alpha_1 - \alpha_2} \, \overline{\chi}^2 + \left[-\delta_u^d - \left(\mu_u^d - \frac{\beta_1 + \beta_2}{1 - \alpha_1 - \alpha_2} x_0 \right) \right] \, \overline{\chi} - \delta_u^d - \mu_u^d = 0.$$

Replacing numerical values in the above equation and computing the Jacobian at the equilibrium points, we obtain solutions $\chi_{1,2}$ that are located at $|\chi_1| > 1$ and $|\chi_2| \leq 1$: they characterise unstable and (locally) stable dynamics, respectively. Unfortunately, solely the unstable equilibrium point can be modified by varying parameters μ_u^d or δ_u^d. In other words, when the frequency signal enters the domain Λ_u^d of the distribution, the population of panels will disconnect, regardless of the parameter values. Therefore, one can only reduce δ_u^d, thus effectively reducing the chance that the disconnection begins.

B Models for Heterogeneous Populations of Solar Panels

In this section we analyse the difference between two approaches to describe a heterogeneous population of solar panels. We focus on a population composed by two clusters: let us define x_1 and x_2 as the probability of being ON of the two clusters, respectively. Recall from Eqn. (1) the dynamics of $x(k)$ and let us consider solely $x(k+1) = a(k)x(k)$. We present two approaches to describe the clusters, considering them independent of each other, namely

$$x_1(k+1) = \int_{A_1} p_1 \cdot x_1(k), \qquad x_2(k+1) = \int_{A_2} p_2 \cdot x_2(k), \tag{11}$$

or by including them into a single variable x_T as

$$x_T(k+1) = \left[c_1 \int_{A_1} p_1 + c_2 \int_{A_2} p_2 \right] x_T(k), \tag{12}$$

where $c_1, c_2 \in [0,1]$ represent the contribution of the two populations, and $c_1 + c_2 = 1$; $\int_{A_1} p_1$ and $\int_{A_2} p_2$ represent integrals over regions corresponding to x_1 and x_2, and where p_1 and p_2 represent the distribution concerning x_1 and x_2, respectively. Considering Eqn. (11), let us define the weighted sum $\bar{x}$ as

$$\bar{x}(k) = c_1 x_1(k) + c_2 x_2(k), \tag{13}$$

where c_1 and c_2 derive from Eqn. (12). The $\mathcal{L}_1$-norm of their difference defines the aggregation error $e_A(k)$

$$\begin{aligned} e_A(k+1) &= |x_T(k+1) - \bar{x}(k+1)| = \\ &= \left| \left[c_1 \int_{A_1} p_1 + c_2 \int_{A_2} p_2 \right] x_T(k) - c_1 x_1(k+1) - c_2 x_2(k+1) \right|. \end{aligned}$$

To ease the notation, define $c_1 \int_{A_1} p_1 := \gamma_1$ and $c_2 \int_{A_2} p_2 := \gamma_2$. Substituting x_1 and x_2 from Eqn. (12), $e_A(k+1)$ becomes

$$|\gamma_1 (x_T(k) - x_1(k)) + \gamma_2 (x_T(k) - x_2(k))| \leq \gamma_1 + \gamma_2.$$

Notice that $e_A(k) = 0$ if and only if $x_1(k) = x_T(k) = x_2(k)$. Recall that x_1 and x_2 denote the active portion of cluster 1 and 2, respectively. If the two clusters are non-coincident x_1 and x_2 assume the same value only when $x_1 = 1 = x_2$ or $x_1 = 0 = x_2$, namely within the safe set on the unsafe set. Frequency values in between the safe set and the unsafe set cause the two variables to have different value, thus $e_A > 0$. Analyse now the worst case scenario, i.e. when $x_1 = 0$ and $x_2 = 1$, and the error e_A takes its maximum value. If variable $x_1 = 0$, given the feedback nature of the interconnection between panels and network, and from Eqn. (11), we must have $\int_{A_1} p_1 = 0$. In this case, the error becomes

$$e_A(k+1) = |\gamma_2 (x_T(k) - x_2(k))| \leq \gamma_2 < 1.$$